ACS APPLIED NANO MATERIALS

www.acsanm.org Article

Direct Metal-Free Growth and Dry Separation of Bilayer Graphene on Sapphire: Implications for Electronic Applications

Sivasakthya Mohan, Dmitry Kireev, Shanmukh Kutagulla, Nicholas Ignacio, Yuqian Gu, Hugo Celio, Xun Zhan, Deji Akinwande, and Kenneth M. Liechti*

Cite This: *ACS Appl. Nano Mater.* 2023, 6, 19018−19028 Read Online

ACCESS | Metrics & More | Article Recommendations | Supporting Information

ABSTRACT: The rate at which graphene is used in different fields of science and engineering has only increased over the past decade and shows no indication of saturating. At the same time, the most common source of high-quality graphene is through chemical vapor deposition (CVD) growth on copper foils with subsequent wet transfer steps that bring environmental problems and technical challenges due to the compliance of copper foils. To overcome these issues, thin copper films deposited on silicon wafers have been used, but the high temperatures required for graphene growth can cause dewetting of the copper film and consequent challenges in obtaining uniform growth. In this work, we explore sapphire as a substrate for the direct growth of graphene without any metal catalyst at conventional metal CVD temperatures. First, we found that annealing the substrate prior to growth was a crucial step to improve the quality of graphene that can be grown directly on such substrates. The graphene grown on annealed sapphire was uniformly bilayer and had some of the lowest Raman D/G ratios found in the literature. In addition, dry transfer experiments have been performed that have provided a direct measure of the adhesion energy, strength, and range of interactions at the sapphire/graphene interface. The adhesion energy of graphene to sapphire is lower than that of graphene grown on copper, but the strength of the graphene−sapphire interaction is higher. The quality of the several centimeter scale transfer was evaluated using Raman, SEM, and AFM as well as fracture mechanics concepts. Based on the evaluation of the electrical characteristics of the graphene synthesized in this work, this work has implications for several potential electronic applications.

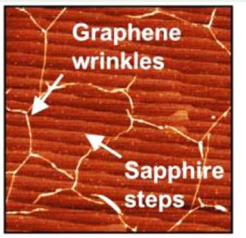

(i) Annealing sapphire prior to growth improves graphene quality.

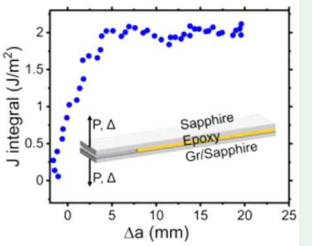

(ii) Direct measurement of graphene-sapphire interactions during centimeter-scale dry transfer provides a quality control metric.

KEYWORDS: *graphene growth, dry transfer, sapphire, adhesion strength, adhesion energy*

1. INTRODUCTION

Two-dimensional (2D) materials have been highly researched in the past two decades due to their promise of extraordinary strength as well as optical, thermal, mechanical, and electronic properties.[1−3] As a pioneer 2D material to be mechanically exfoliated,[4] there has been a vast school of research on graphene. Despite this, there are still challenges preventing the successful transition of graphene from laboratory to industrial applications. These include obtaining wafer-scale graphene with high crystallinity that can be transferred to a suitable substrate with minimal contamination.[5−7]

The most common approach for growing graphene on a large scale is chemical vapor deposition (CVD). A lot of research has been conducted to elucidate the mechanisms associated with growing graphene on copper foil.[8−11] However, for graphene to be translated into commercial applications, any graphene that is grown on copper foil must be transferred to a suitable substrate such as SiO_2/Si. To date, wet transfer has been the preferred approach, in which a sacrificial polymer is first coated on the graphene, followed by copper etching, which is a highly corrosive and environmentally unfriendly process. While this process has proven effective in the large-scale transfer of monolayer graphene from copper, there are still some difficulties such as long processing times, unwanted doping, and harmful etchants contaminating and damaging the graphene film during the transfer process.[12] To this end, a dry transfer method was developed[13] for transferring graphene from copper foil. This method not only eliminates the use of chemical etchants but also provides a way to directly measure the adhesion energy at the graphene/copper interface. Table S3 provides a summary of results from previously reported dry transfer experiments involving graphene. Na et al.[14] further showed that the rate of delamination was key to obtaining successful transfer from the desired interface under nominally mode I fracture conditions. More recently, adhesion energy measurements between copper

Received: July 28, 2023
Accepted: September 28, 2023
Published: October 12, 2023

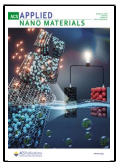

https://doi.org/10.1021/acsanm.3c03533
ACS Appl. Nano Mater. 2023, 6, 19018−19028

Scheme 1. Use of Thermal Annealing to Carry out the High-Quality, Metal-Free Growth of Bilayer Graphene on Sapphire and the Subsequent Dry Separation to Directly Measure the Adhesion Energy and Strength of the Graphene/Sapphire Interface

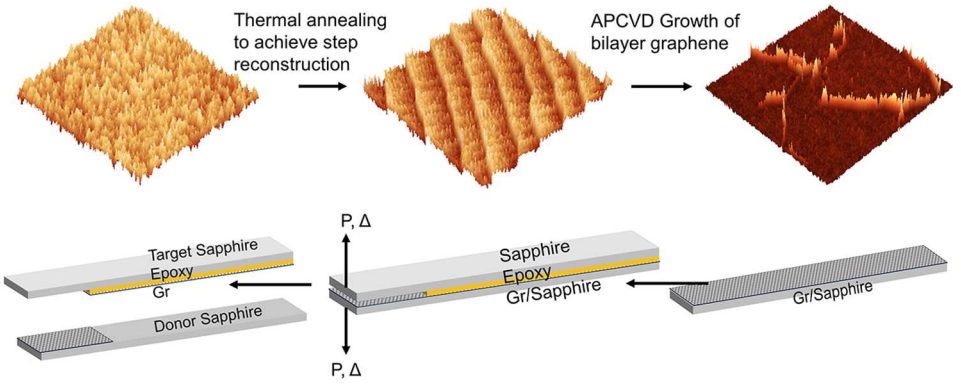

foil and graphene were obtained using roll-to-roll dry transfer by Hong et al.[15] to transfer large area graphene from copper foil using PVA. Adopting the dry transfer method for copper foil might present some challenges due to the compliance and lack of mechanical rigidity of the foils. For this reason, thin copper films deposited on SiO_2/Si were used.[16] However, at the high growth temperatures (~1000 °C), dewetting of copper (which has a melting point of 1085 °C) is a commonly encountered problem.[17,18] Besides, subjecting SiO_2/Si to such high temperatures usually damages the quality of oxides, facilitates metal diffusion, and restricts the back end of the line (BEOL) implementation. To counter some of these challenges, substrates other than copper have been considered for the metal-free growth of graphene.[19−22] Epitaxial growth on silicon carbide (SiC) has been studied,[23−25] but the process is too expensive with a very niche range of applications. Directly growing graphene on silicon wafers has also been considered,[26] but the resulting graphene films are not continuous over large areas. The use of sapphire (Al_2O_3), for the direct growth of very high-quality graphene, is a relatively new emerging area of research. Table S2 summarizes some of the growth parameters and key results obtained from the direct growth of graphene on sapphire from previous literature. Following methane decomposition at high temperatures, the carbon atoms nucleate, and graphene flakes are formed in the gaseous environment and are subsequently deposited on the sapphire substrate.[27] Previous reports indicate that growing high-quality graphene on sapphire requires very high temperatures (~1425−1525 °C),[28] additional surface pretreatments like annealing using different gaseous environments,[29] or the use of modified plasma-enhanced CVD equipment.[30] Mishra et al.[29] reported that a hydrogen etching step was required prior to graphene growth to obtain an aluminum-rich surface reconstruction on sapphire, suitable for growing wafer-scale graphene. In another study by Li et al.[30] polycrystalline copper foil placed on sapphire was first converted into a single-crystal copper via annealing. Graphene was then grown at the interface between copper and sapphire by multicycle plasma etching-assisted CVD. While some of these studies[29,30] have demonstrated the direct growth of fab-compatible graphene on sapphire, there have been very few works that have investigated the interfacial properties between the as-grown graphene and sapphire.[31]

In this study, thermal annealing has been employed as a surface treatment step prior to graphene growth. The substrates were annealed at sufficiently high temperatures and for long durations for the formation of well-defined atomic steps on the surface. The formation of these steps is crucial to the improved quality of graphene, as has been previously demonstrated[32] for the epitaxial growth of highly aligned MoS_2. The graphene grown on the annealed substrates had $I_{D/G}$ ratios as low as 0.14 and was uniformly bilayer in nature. Following the growth, nominally mode I fracture experiments have been performed for the successful dry transfer of graphene from its sapphire growth substrate, while the adhesion energy, strength, and range of the interaction between graphene and sapphire have been measured directly. The measured interface toughness values were relatively higher than what could be expected for pure van der Waals interactions, but they were significantly lower in comparison with graphene/copper adhesion energies. These findings provide valuable insights for commercializing the large-area dry transfer of graphene from its growth substrates. Mobilities have been extracted from the synthesized and transferred graphene, which show promise for potentially using graphene in electronic applications.

2. MATERIALS AND METHODS

2.1. Growth of Graphene. Four inch, single side polished, R-plane (1102) sapphire wafers (0.5 mm thick) were purchased from University Wafers. The samples were cleaned with acetone and isopropyl alcohol. The cleaned samples were then annealed in air for 4 h at 1100 °C. Immediately following annealing, the samples were loaded into a 1 in. horizontal tube furnace. The temperature of the furnace was ramped to 1050 °C. Argon (200 sccm), hydrogen (80 sccm), and methane (30 sccm) were used during growth. After a dwell time of 3 h, the gas flows were stopped, and the furnace was cooled to room temperature. The furnace was maintained at atmospheric pressure during graphene growth.

2.2. Characterization of the As-Grown Graphene. Post growth, the samples were characterized using Raman, SEM, and AFM. A Renishaw Raman spectrometer with laser wavelength of 532 nm was used for spectroscopy. SEM was conducted using an FEI Quanta 600 field emission scanning electron microscope with an electron voltage of 20 kV and emission current of 80 μA. An NX10 Park AFM was used at a scan rate of 1 Hz for obtaining the AFM micrographs. The cross-sectional high-resolution transmission electron microscopy (HRTEM) images were obtained by using a JEOL NEOARM equipped with a probe corrector for STEM and an EDS. An accelerating voltage of 200 kV was used to acquire the images. A 50 nm thick Au film was deposited by an e-beam evaporator, and an additional 2 μm thick ion beam-induced Pt film was deposited to prevent FIB damage and charging. An electron transparent lamella was prepared with a Thermo Scientific Scios DualBeam focused ion beam (FIB)/scanning electron microscope (SEM) system.

https://doi.org/10.1021/acsanm.3c03533
ACS Appl. Nano Mater. 2023, 6, 19018−19028

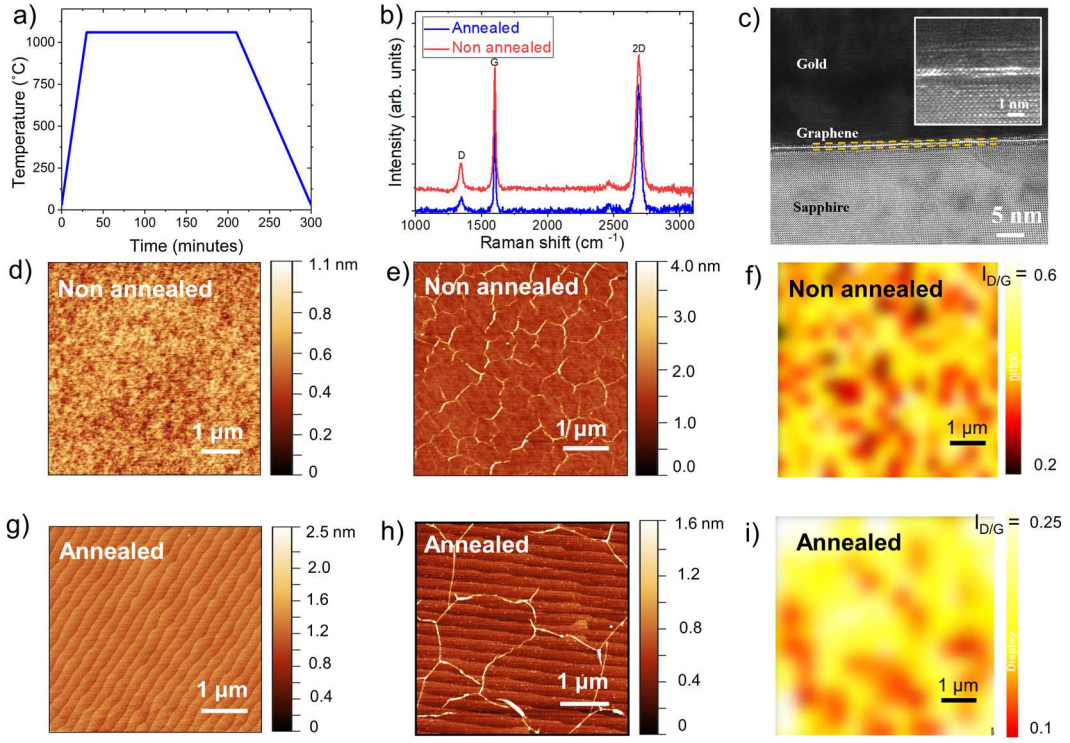

Figure 1. (a) Temperature profile for the growth process. (b) Raman spectra taken on graphene grown on nonannealed and annealed sapphire. (c) High-resolution transmission electron microscopy image of as-grown graphene on annealed sapphire (inset showing a magnified image of the graphene layers with an interlayer distance of 0.3 nm). (d) AFM of the nonannealed surface of sapphire. (e) AFM of graphene on nonannealed sapphire shows wrinkles arising from differences in coefficient of thermal expansion between the film and substrate. (f) Raman map of $I_{D/G}$ on graphene grown on nonannealed sapphire. (g) AFM of the annealed surface of sapphire. (h) AFM of graphene grown on annealed sapphire shows a reduction in wrinkle density. (i) Raman map of $I_{D/G}$ on graphene grown on annealed sapphire. Line profiles of the AFM images are provided in Figure S13.

2.3. Electrical Characterization. Immediately after the sapphire/graphene slab is placed on top of the gel, which is self-adhesive, electrical characterization was performed using the Keysight B2902A Precision Source/Measure Unit (SMU). The gate potential (V_G) was connected to the sintered Ag/AgCl at the bottom of the gel (2360 3M) and swept in the range from −1 to +1. The drain−source potential (V_{DS}) was kept at 100 mV.

2.4. Preparation of Laminated Beam Specimens. Samples used for the mechanical delamination experiment were first diced into strips of dimensions 55 mm × 5 mm. The donor sapphire with graphene was then sandwiched to a target sapphire (C-plane (0001) from Ad Value Technology) strip of identical dimensions by using a thin layer of epoxy. Masterbond epoxy EP 30 was used in the sandwich specimens. The specimens were cured in a convection oven at 100 °C for 2 h. The thickness of epoxy was obtained from the difference in the total thickness before and after curing. For the specimens used in the current study, the thickness of epoxy was 15−20 μm. Post curing, loading tabs containing DIC (digital image correlation) targets were glued to the specimens using commercial Superglue.

3. RESULTS AND DISCUSSION

3.1. Annealing to Improve Growth Quality. Two types of graphene growth procedures were performed to study the effect of annealing the substrates prior to the APCVD growth process. In the first growth procedure, after an initial cleaning using acetone and IPA, the sapphire substrates were directly loaded into a horizontal tube furnace that was used for graphene growth. The temperature profile shown in Figure 1a was used for the growth (further details of the growth recipe are provided in the Methods section). In the second type of growth, post cleaning, the substrates were first annealed in air at 1100 °C for 4 h. Immediately following annealing, the substrates were loaded into a horizontal tube furnace for graphene growth using the same temperature profile presented in Figure 1a. In both types of growth, the CVD was performed at atmospheric pressure and the growth temperature was maintained at 1050 °C.

Raman spectroscopy and scanning electron and atomic force microscopy were used to characterize the samples following growth. The Raman signature of graphene for the current samples, composed of the D peak (1340 ± 1.7 cm^{-1}), G peak (1595 ± 1.6 cm^{-1}), and 2D peak (2685 ± 1.8 cm^{-1}), provides information on the quality and number of layers of the as-grown graphene.[33] As confirmed by the $I_{2D/G}$ ratio in the Raman spectra of the as-grown graphene samples (Figure 1b), bilayer graphene is obtained on sapphire following our current growth recipe. The AFM images on sapphire show the formation of a well-defined surface consisting of atomic steps following high temperature annealing (Figure 1g) without much variation in the surface roughness, when compared with the as-received sapphire (Figure 1d). It is believed that the formation of these surface steps during annealing is crucial to improving the crystallinity of the as-grown graphene, as clearly evidenced by the reduction in the average $I_{D/G}$ ratio. The average $I_{D/G}$ ratio decreased by about 50% to a value of 0.14 on the samples whose sapphire surfaces were annealed prior to growth. This is one of the lowest reported values in the literature for the direct, metal-free growth of graphene on sapphire at conventional metal-CVD temperatures. Large-scale Raman spectroscopy mapping revealed that about 60% of the sample area had an $I_{D/G}$ ratio of 0.15−0.22 (Figure 1i), when the growth substrates were preannealed. The $I_{D/G}$ ratio is an important indicator of the graphene quality as it has been used to characterize the defect densities in the graphene

https://doi.org/10.1021/acsanm.3c03533
ACS Appl. Nano Mater. 2023, 6, 19018−19028

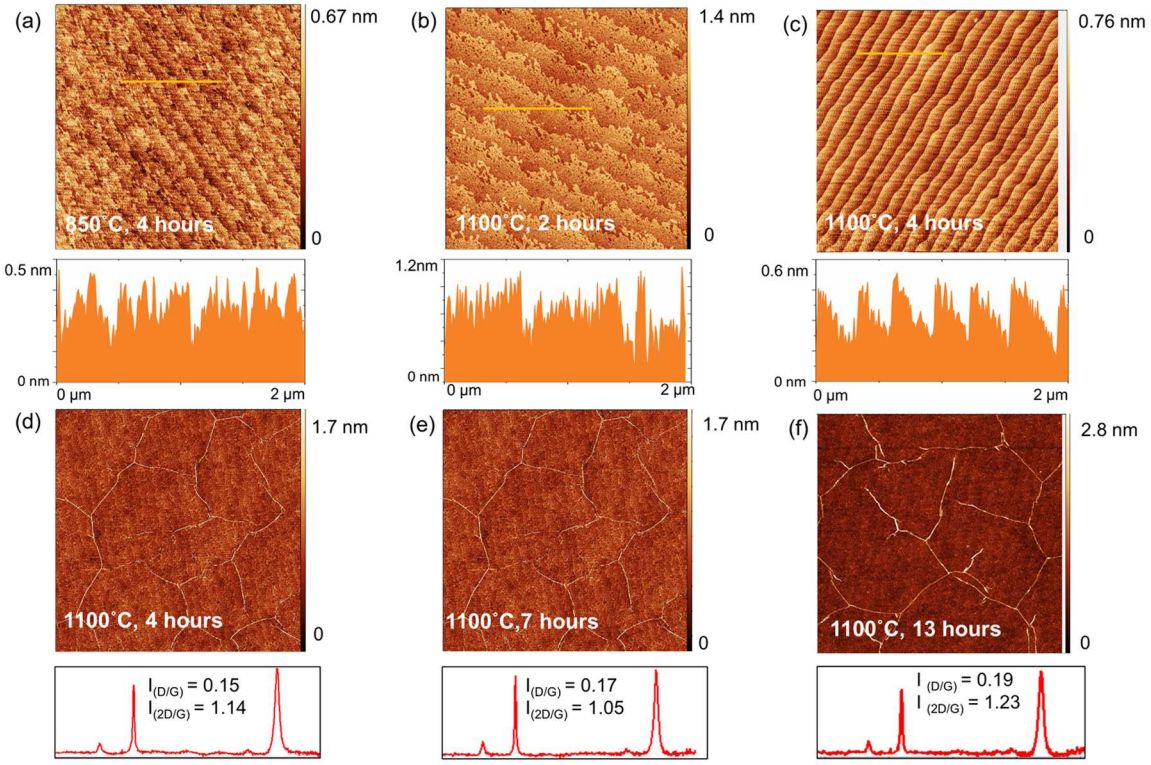

Figure 2. (a–c) AFM images (5 μm × 5 μm) on annealed sapphire, showing the surface step formation on the sapphire substrates post annealing at different times and temperatures as indicated. (d–f) AFM images (10 μm × 10 μm) and Raman spectra of the synthesized graphene/annealed sapphire. The sapphire substrates were all annealed at 1100 °C for different times as indicated in the images.

structure and is related to the graphene grain size.[34] As has been presented, the graphene on preannealed sapphire substrates has lower D/G ratios pointing toward fewer defects and an improvement in the crystallinity of the as-grown graphene. This agrees with previous works[32] where it has been shown that the crystallinity of synthesized 2D materials such as MoS_2 has improved when the sapphire substrates are preannealed due to a preferred alignment of the MoS_2 flakes along the well-defined atomic steps on the surface.

The white ridges present in the AFM images of as-grown graphene (Figure 1e,h) have been understood as wrinkles that are formed during the cooling phase of the CVD growth due to differences in the coefficient of thermal expansion between graphene and sapphire. The presence of these wrinkles everywhere on the sample pointed to the continuous coverage of the graphene films obtained in this growth. One of the issues with CVD graphene is the presence of wrinkles that arise due to the differences in the thermal expansion coefficients, as wrinkles can affect electron transport properties.[35] When the substrates are preannealed, there is a clear reduction in the wrinkle density which is a promising step in improving the graphene quality. High-resolution transmission electron microscopy (HR-TEM) images of the as-grown graphene on annealed sapphire (Figure 1c) showed the presence of the bilayer graphene with an interlayer distance of ~0.3 nm, which agrees well with previous reports from the literature.[36] The number of layers of graphene was further inferred from the Lorentzian deconvolution of the 2D peak of the Raman spectrum taken at several points on the sample. Four Lorentzian curves were consistently required to obtain the best fit of the 2D peak (Figure S6). Moreover, the average full width at half-maximum of the 2D peak was 43.2 ± 0.6 cm^{-1}. Large-area Raman maps (Figure S7) taken at different locations on the sample confirm that the Raman $I_{2D/G}$ ratio is between 0.9 and 1.3 over the measured area. These findings further support the claim that the as-grown graphene is bilayer.[33] SEM and optical images for graphene on annealed sapphire (provided in Figures S1 and S16) show the continuity of the graphene films. XPS measurements (Figure S2) on the as-grown graphene show the presence of C 1s and Al 2p peaks. They do not provide information on any chemical interactions or molecular bonds that are present between the graphene and sapphire. R-plane sapphire was used in this work, as it provided the best graphene quality in terms of the Raman $I_{D/G}$ ratio with the current growth recipe. The Raman characterization data for the as-grown graphene on C-, R-, and A-plane sapphire wafers have been summarized in the Supporting Information (Figure S15).

3.2. Optimization of Growth and Annealing Parameters. The growth process for obtaining bilayer graphene on sapphire was optimized in the following manner. The mass flow rates of the gases and the reaction dwell time t were adjusted to obtain complete coverage of graphene on the sapphire substrates, which was validated using Raman spectra and SEM images. SEM images taken with varying dwell times (see Figure S8) indicate that at 180 min we obtain complete coverage, and the corresponding Raman spectra and maps confirm the presence of uniform bilayer graphene. As the dwell time exceeds 180 min, we notice the presence of discontinuous adlayer flakes. The current growth is performed in a horizontal tube, hot wall reactor furnace where the temperature of the gases over the substrate is relatively high, causing the nucleation of several large carbon clusters at high growth temperatures.[37] This typically results in the growth of few-layer graphene more easily than does single-layer graphene. An exact control of the growth parameters

https://doi.org/10.1021/acsanm.3c03533
ACS Appl. Nano Mater. 2023, 6, 19018−19028

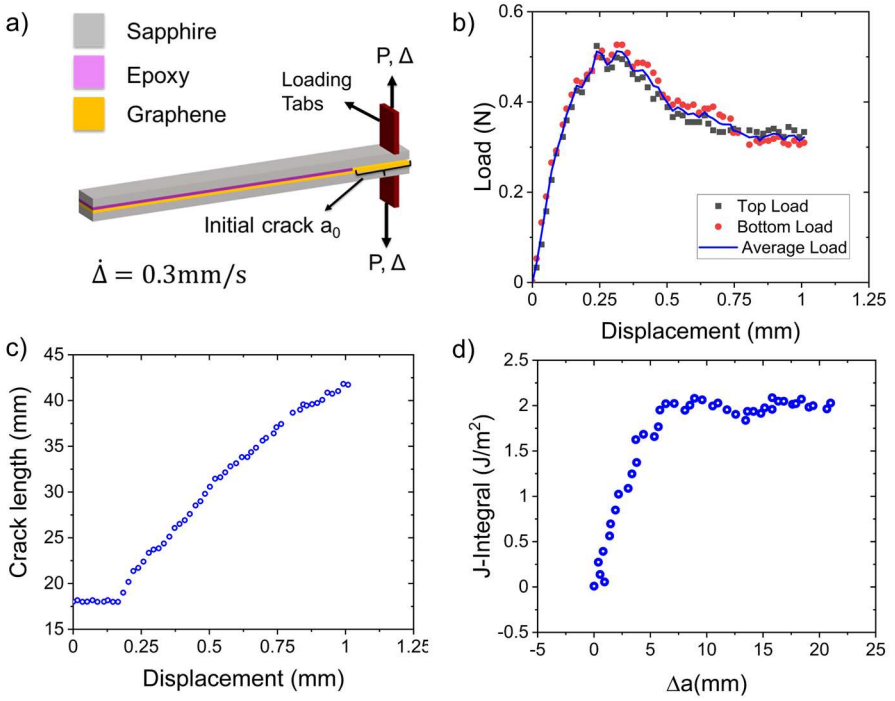

Figure 3. (a) Schematic of a sample prepared for dry transfer of graphene on sapphire. (b) Measured load−displacement response. Load signals from top and bottom cells and their average are plotted against the total displacement at the loading point. (c) Crack growth plotted as a function of total displacement. (d) Resistance curve (plot of *J*-integral as a function of change in crack length Δa).

such as time, temperature, and the mass flow control of the precursor gases is thus important for obtaining a precise number of graphene layers. This contrasts with furnaces that rely on other heating methods (such as electromagnetic induction) where the substrate is shielded from very high temperatures and the growth happens without the presence of large carbon clusters. In the current growth recipe that we adopted, we have been able to grow uniform bilayer graphene on sapphire, as evidenced by Raman spectroscopy and high-resolution transmission electron microscopy of the cross section.

The ratio of CH_4/Ar was fixed at 30/200 sccm following a growth recipe outlined elsewhere.[27] The effect of hydrogen was studied by varying the H_2/Ar mass flow rates as 50/200, 75/200, and 100/200. From the SEM images (Figure S8), we see that at the lower H_2 flow rates, the resulting graphene flakes provide only partial coverage over the substrates, and as the H_2 concentration is increased to 1:2, the hydrogen rapidly etches away the graphene domains. This is in line with the two well-known roles that hydrogen typically plays in the chemical vapor deposition growth of graphene:[38] (1) providing catalytic decomposition of the hydrocarbon source and (2) an etching agent that provides control over the morphology of the graphene domains.

The parameters (time and temperature) of annealing were chosen to obtain uniform steps over the entire sapphire surface. The evolution of the step morphology on R-plane sapphire surfaces has been studied by Komurasaki et al.,[39] where it was shown that the uniformity of the steps improved with an increase in annealing time and temperature. In our current work, two temperatures were explored for annealing the sapphire prior to the growth of graphene: 850 and 1100 °C. (The furnace is programmed to allow only certain fixed temperature profiles for the annealing, preventing a more thorough exploration into the influence of parameters on the surface step evolution.) At 850 °C, with a 4 h annealing, a rough terrace structure is formed but with many islands and voids. The uniformity of the step structure improved when the annealing was performed for 2 h at a higher temperature of 1100 °C, with still some discontinuities on the step edges. These were largely eliminated resulting in straight step edges when the time was increased to 4 h. The AFM images and line profiles of these cases are presented in Figure 2a−c. Beyond 4 h, there was no visible improvement in the quality of graphene that was synthesized on the annealed sapphire. Figure 2e,f shows that even with an increased duration of 7 and 13 h, there is no further reduction in the $I_{D/G}$ or in the wrinkle density.

3.3. Measurement of Graphene/Sapphire Interactions. For the dry transfer experiments, graphene was grown on sapphire strips measuring 55 mm × 5 mm tailored specifically for dry transfer. Laminated beam specimens (Figure 3a) were prepared by sandwiching the as-grown graphene on sapphire with another sapphire strip through a thin layer of low-viscosity epoxy (Masterbond EP 30). By careful specimen preparation, the thickness of the epoxy was consistently in the range of 15−20 μm. The target substrate was chosen as sapphire for symmetry and to provide a nominally Mode I fracture (tensile) condition at the crack front. The epoxy was applied for about three-fourths of the total length of the strip to provide an initial crack (a_0) for delamination. Epoxy curing was performed in a convection oven at 100 °C for 2 h. Post curing, a wedge was driven though the initial blunt crack or bimaterial corner between the epoxy terminus and the graphene, in order to create a sharp crack tip and thereby avoid blunting effects. Loading tabs containing digital image correlation (DIC) targets were glued to the specimen, and the specimen was installed in a dual actuator loading device. Using two independently controlled actuators, this device provides a full range of fracture mode mixes or combinations of tension and shear. In the current study, tensile

https://doi.org/10.1021/acsanm.3c03533
ACS Appl. Nano Mater. 2023, 6, 19018−19028

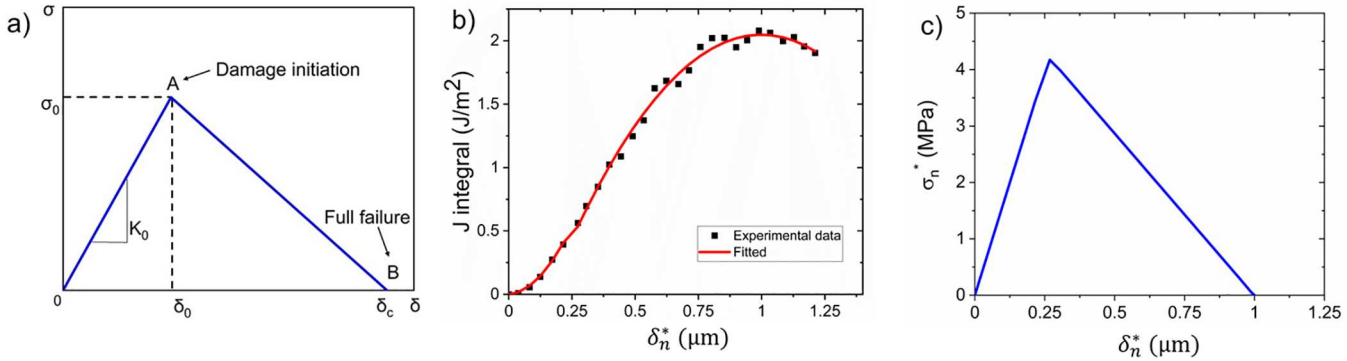

Figure 4. (a) Bilinear traction−separation model often used in characterizing the development of damage at the interface. (b) *J*-integral plotted as a function of the crack tip opening displacement. (c) Extracted bilinear traction−separation relation obtained from the first derivative of the *J*-integral with respect to the normal crack tip opening displacement.

interactions were excited by setting the ratio of the top and bottom end-displacements to 1 by prescribing the same displacement rate (0.3 mm/s). Load signals from the top and bottom load cells were collected with a Lab View program while end-displacements and rotation angles were obtained used digital image correlation. Post transfer, the fracture surfaces were characterized using Raman spectroscopy, SEM, and AFM.

A typical load *vs.* end-displacement response is provided in Figure 3b. The two load cell signals were suitably consistent during the experiment, thereby confirming the symmetric loading of the laminated beam specimen. The average load value at any applied displacement value was used in subsequent processing of the data. The load increased linearly to approximately 0.45 N until the onset of interfacial damage. The slope of the response then decreased to zero as the cohesive zone developed fully. This was followed by a steady decrease in the load as the cracks grew along the interface. Raman spectra taken on both fracture surfaces at various locations along their length revealed that the delamination occurred between graphene and sapphire, as will be discussed in the next section. The initial crack length was determined before the experiment, as the optical transparency of the sapphire strips allowed it to be precisely determined following the insertion of a wedge in order to provide a sharp crack.

A beam on elastic foundation model[40] was used to model the initial load−displacement response as follows:

$$P = \frac{3\Delta \bar{E}_1 I_1}{2a^3}\left(1 + \frac{3}{\lambda a} + \frac{3}{(\lambda a)^2} + \frac{3}{2(\lambda a)^3}\right)^{-1} \quad (1)$$

Here P denotes the average load, Δ is the total displacement of the loading points, a is the crack length at any point of the experiment, $I_1 = \frac{bh^3}{12}$ refers to the cross-sectional moment of inertia about the neutral axis of each beam, b is the specimen width (5 mm), and h is the thickness of the sapphire (0.5 mm). $\bar{E}_1$ refers to the plane strain Young's modulus of the sapphire, given by $\frac{E_1}{1-\nu_1^2}$ where ν_1 is its Poisson's ratio and $\lambda = \left(\frac{6K_0}{\bar{E}_1 {h_1}^3}\right)^{1/4}$. The quantity K_0 is the stiffness of the elastic foundation, which is determined from the initial stiffness of the load−displacement response and the initial crack length (i.e., $a = a_0$) via eq 1. A three-point flexural test had been performed on the sapphire to obtain its strength (450 MPa) and a Young's modulus of 320 GPa (details in Figure S11 and Table S1).

Beyond the initial crack length, the current crack length a at any particular applied displacement was obtained from load−displacement data and the determined foundation stiffness using the following relation:

$$a = \frac{1}{\lambda}\left[\left(\frac{3\lambda^3 \bar{E}_1 I_1 \Delta}{2P} - \frac{1}{2}\right)^{1/3} - 1\right] \quad (2)$$

Finally, the *J*-integral at any point in the experiment is given by

$$J = \frac{12P^2}{\lambda^2 \bar{E}_1 {b_1}^2 {h_1}^3}\left[\frac{3\lambda^3 \bar{E}_1 I_1 \Delta}{2P} - \frac{1}{2}\right]^{2/3} \quad (3)$$

The variation of the *J*-integral as a function of the change in crack length Δa, which is also known as the resistance curve (Figure 3d), increased during the rising portion of the load−displacement curve, before transitioning to a steady state value of 1.98 J/m^2 when the cohesive zone had fully developed. This remained constant for about 15 mm of delamination and is the adhesion energy or toughness of the interaction between graphene and sapphire. It is lower than the adhesion energy of 6 J/m^2 of the interface between graphene and copper foil determined in a previous work.[14] The adhesion energy obtained from our experiments compares well with the previously reported adhesion energy of 1.45 J/m^2 that was measured using a nanoscratch AFM experiment.[31]

The cohesive interactions at the graphene/sapphire interface were modeled by using a bilinear traction−separation relation (schematic representation in Figure 4a). The interface initially opens elastically with the stiffness K_0, until point A, where the traction reaches the strength of the interface σ_0 at a corresponding value of the interface separation, δ_0. At this point, damage initiates and continues to progress as the separation increases while the stress decreases linearly, until finally the interface is fully fractured at point B.

For the traction−separation relation $\sigma(\delta)$, the adhesion energy is obtained by integrating it over the range (δ_c) of the interaction:

$$\Gamma = \int_0^{\delta_c} \sigma(\delta)\, \mathrm{d}\delta \quad (4)$$

The parameters of the traction−separation relation were determined using direct measurements of loads and displacements. The normal crack tip separation was obtained[40] from the beam-on-foundation analysis as

https://doi.org/10.1021/acsanm.3c03533
ACS Appl. Nano Mater. 2023, 6, 19018−19028

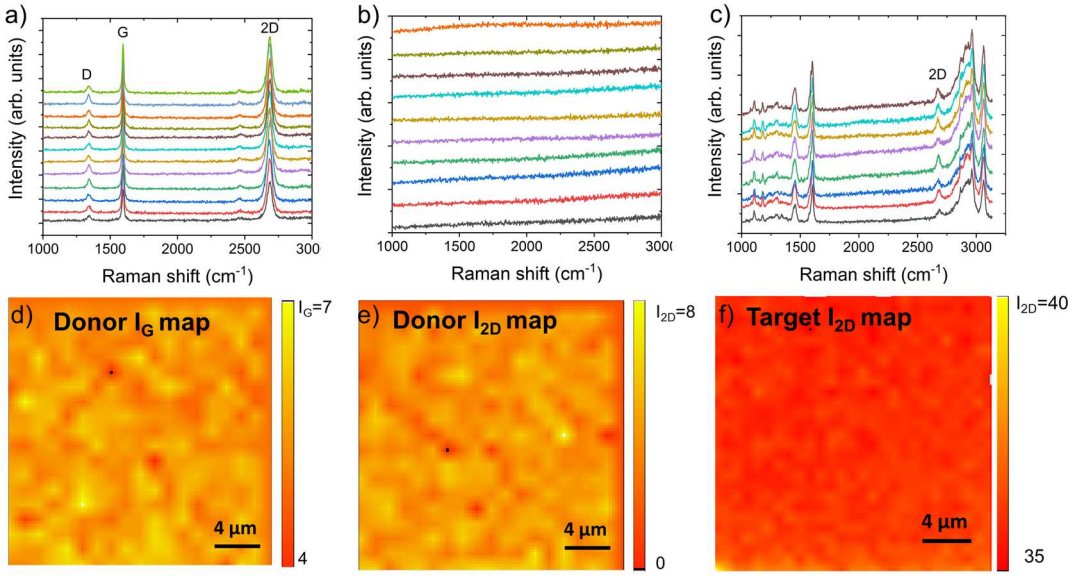

Figure 5. Point-to-point Raman spectra on the (a) donor sapphire prior to transfer, (b) donor sapphire post transfer, and (c) target sapphire post transfer. Raman intensity post transfer: (d) map of I_G peak on donor, (e) map of I_{2D} peak on donor, and (f) map of I_{2D} peak on target.

Table 1. Summary of Adhesion Energy and Strength Obtained from the Measured Load−Displacement Responses of the Different Samples

	K_0 (N/m^3)	epoxy thickness (μm)	initial crack length a_0 (mm)	transfer length $\Delta a = a - a_0$ (mm)	adhesion energy (J/m^2)	strength (MPa)	range of interactions (μm)
1	9.8×10^{12}	20	17	20	2.01	4.1	1
2	4.0×10^{12}	20	14	18	1.89	3.32	1.36
3	5.6×10^{12}	20	12	18	2.21	3.7	1.5
4	4.8×10^{12}	15	11	25	2.86	4.16	1.67

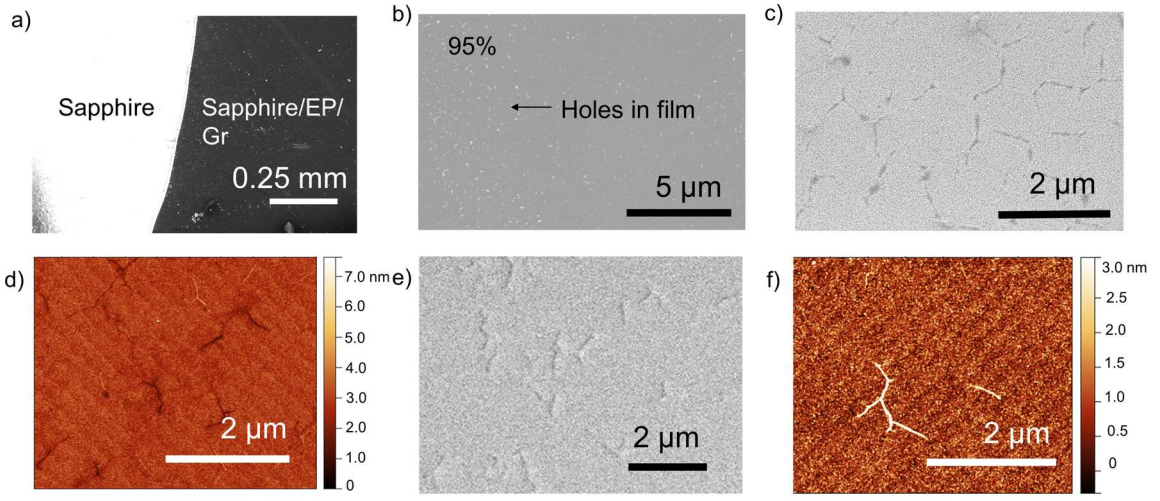

Figure 6. (a−d) Target post transfer diagnostics: (a) Low-magnification SEM image of crack front shows distinction between bare sapphire and graphene covered epoxy/sapphire. (b) Yield of graphene transfer characterized from SEM on target substrate. (c) High-magnification SEM image. (d) AFM image. (e, f) Donor post transfer diagnostics: (e) high-magnification SEM image, (f) AFM image.

$$\delta_0^* = \frac{P(1+\lambda a)}{\bar{E}_1 I_1 \lambda^3} \tag{5}$$

The J-integral (eq 3) is then tracked as a function of the normal crack tip opening (eq 5), and the normal traction at the initial crack tip (Figure 4c) is obtained as the first derivative of the J-integral with respect to the normal crack tip opening displacement:

$$\sigma_0^* = \frac{\partial J}{\partial \delta_0^*} \tag{6}$$

The strength of the graphene/sapphire interface was determined (Figure 5a) as 4.1 MPa, and the corresponding interaction range was 1 μm. This strength value and relatively long interaction range suggest that there could be mechanisms other than simple van der Waals interactions occurring between graphene and sapphire. Previous studies[31] have shown the

https://doi.org/10.1021/acsanm.3c03533
ACS Appl. Nano Mater. 2023, 6, 19018−19028

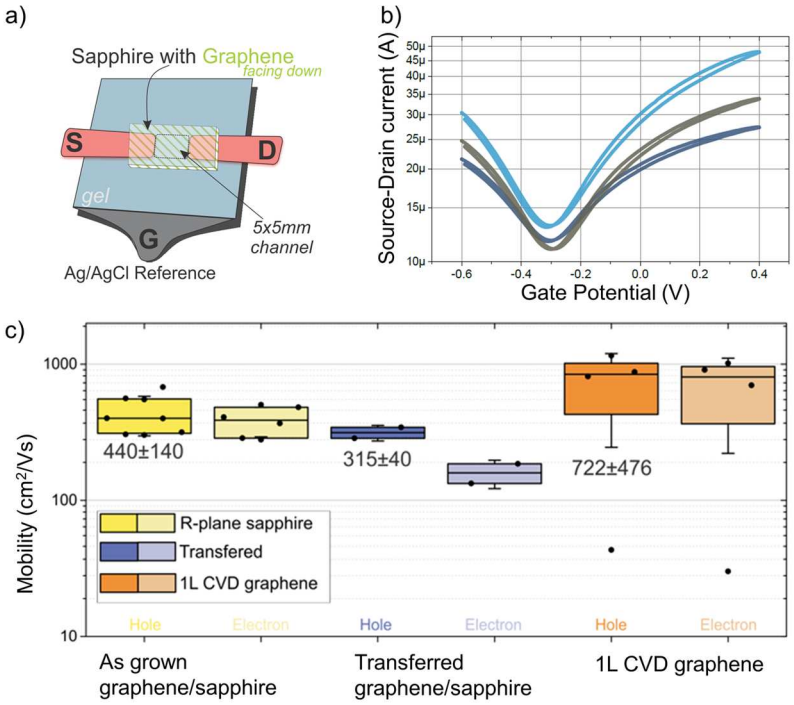

Figure 7. (a) Schematic of the gel-based nondestructive and low-cost graphene performance characterization setup, consisting of a gel (gray blue), underlying Ag/AgCl reference electrode (black), source and drain metal contacts (pink), and graphene/sapphire slab placed graphene facing down. Typically, the channel length and width are set to 5 mm each. (b) Three $I_{DS}-V_{GS}$ characterization curves of the graphene grown on sapphire. (c) Statistical distribution of the device performance in terms of electron and hole mobility of the graphene directly grown on sapphire (yellow), transferred from the sapphire (violet), given in comparison to the CVD graphene grown on copper foil and wet-etched, only supported by the PMMA.

presence of a covalent interaction when multilayer graphene is grown directly on sapphire due to an oxygen-rich surface reconstruction and resulting C−O−Al bonds, which could potentially explain the strength values that we obtain in our experiments. It is interesting to observe that even though the as-grown graphene is bilayer, the graphene−graphene interface did not delaminate during the dry transfer. The path of interfacial delamination could be more strongly dictated by the strength of an interface rather than the interface toughness (or adhesion energy).[41] Theoretical experiments using MD simulations have shown that the interlayer strength of bilayer graphene is approximately 1−4 GPa,[42−44] which is orders of magnitude stronger than the experimentally determined graphene/sapphire strength of 4.1 MPa. The interfacial properties obtained from the measured load−displacement responses of different samples are summarized in Table 1 and Figure S14. The current study does not consider the effect of the variation in adhesive forces as a function of the sapphire step orientation.

3.4. Post Transfer Characterization. The donor and target sapphire strips were characterized through a combination of Raman spectroscopy and SEM and AFM microscopy. Raman spectra taken at several points along the donor substrate before transfer (Figure 6a) confirmed the presence of high-quality graphene along the entire length of the strip. The interface of delamination was confirmed as graphene/sapphire because there were no significant graphene peaks present on the donor substrate post transfer (Figure 5b) besides the sapphire peak at 550 cm^{-1}. It is worth noting that Raman still showed the presence of graphene on the donor in the region where no epoxy was applied to provide for initial crack a_0. Raman spectra on the target (Figure 5c) further confirmed that all of the graphene had been transferred onto the epoxy/sapphire. The G peak of the graphene has been deconvoluted from the epoxy peak (Figure S12), and furthermore, the graphene 2D peak can be distinguished clearly from the Raman spectra of the background epoxy, validating that bilayer graphene has been successfully transferred along the entire length of the substrate. Raman mapping was conducted on both donor and target sapphire strips post transfer for areal characterization. There were no significant graphene peaks visible anywhere on the donor, and a nontrivial 2D peak was always found on the epoxy/sapphire. The background signal from epoxy prevents the number of layers of graphene from being directly determined by the Raman $I_{2D/G}$ ratio. However, Lorentzian deconvolution was performed for the 2D peak as before; 4 Lorentz curves were required to obtain the best fit of the 2D peak which confirmed that the experiments yielded transfer of both the graphene layers from the donor sapphire (Figure S9).

In addition, both fracture surfaces were imaged under low and high magnification using SEM and AFM. The absence of any significant charging effects (Figure 6a) on the epoxy during SEM was an additional confirmation of uniform graphene coverage everywhere on the target substrate. The low-magnification SEM image (Figure 6b) reveals the presence of holes in the transferred film caused by bubbles in the epoxy, which may not have been fully removed during the specimen preparation. However, these images still show a high yield of 95% from the dry transfer. The low-viscosity epoxy conformed well to the graphene wrinkles during specimen preparation, as evidenced by the dark lines in the AFM images of the target (Figure 6d), which followed the morphology of the as-grown graphene wrinkles very well. High-magnification SEM and AFM images (Figure 6e,f) exhibited some residual wrinkles that were still present on the donor substrate after transfer. However, the wrinkles are too

https://doi.org/10.1021/acsanm.3c03533
ACS Appl. Nano Mater. 2023, 6, 19018−19028

small for their composition to be identified and resolved by Raman spectroscopy.

3.5. Electrical Characterization of the As-Grown Graphene. In order to evaluate the electrical properties of the large-scale grown graphene, we developed a methodology that allowed us to perform field-effect transistor measurements without actually transferring graphene from the substrate. The method relies on commercially available gel electrodes, consisting of an adhesive hydrogel and an underlying Ag/AgCl electrode (i.e., 3M 2360 red dot series). The gel plays the role of highly conductive electrolyte (hence providing an interface capacitance of 1.4 μF/cm^2), which is an empirical value for field-effect measurements in highly concentrated solutions away from the Dirac point.[45] Two ultrathin adhesive tapes[46] with ∼100 nm thick gold on top is placed on top of the hydrogel, with gold facing up, leaving a 5 mm gap. When the graphene/sapphire slab is placed upside-down, the 5 mm gap between the gold tapes forms the channel length, and the channel width is determined by the graphene piece (see Figure 7a). Applying 100 mV of drain−source voltage (V_{DS}), the drain−source current (I_{DS}) is measured as a function of the gate−source (V_{GS}) potential. The resulting V-shaped response (Figure 7b) classically mirrors the one associated with graphene. It is important to note that, in contrast to graphene transferred by the wet-etch method, the graphene on the growth substrate is n-doped (charge neutrality point is shifted to the left of zero voltage). This could be a result of the graphene itself being slightly n-doped during the growth and the fact that the measurements are made directly on the graphene synthesized on the growth substrate. In contrast, with CVD graphene, it is the transfer that slightly dopes the graphene to p-type, and this is why CVD grown graphene FET sweeps typically show p-type performance.[47] However, when extracting the field-effect mobility, we see an almost 2-fold lower value compared to the monolayer CVD-grown and wet-etched graphene (Figure 7c). We note that the channel size in our measurements is ∼25 mm^2, which is perhaps the reason for even commercial monolayer CVD graphene to feature much lower mobility values than might be expected. Reducing the channel dimensions and building nanoscale transistors reduces the chance of encountering a grain boundary, crack, or a fold. Measuring them in a highly controllable setting would certainly provide a much higher performance metric. However, such highly controlled conditions are not typically encountered in real-world applications. Nonetheless, even at such a large scale, the graphene quality would be highly suitable for biosensing applications, for example.

4. CONCLUSIONS

In summary, high-quality graphene was grown directly on an R-plane sapphire substrate at metal-CVD temperatures through chemical vapor deposition at atmospheric pressure. We have demonstrated that annealing the sapphire at high temperatures prior to growth caused a significant reduction in the graphene $I_{D/G}$ ratio, improved the quality of graphene, and reduced the density of graphene wrinkles. Graphene with an $I_{D/G}$ ratio as low as 0.14 was obtained in our experiments. Cross-section TEM images of the graphene on annealed sapphire, the Raman $I_{2D/G}$ ratio, and the Lorentzian deconvolution of the Raman 2D peaks revealed that the growth process outlined in the current study produces uniform bilayer graphene. Based on evaluation of the electrical characteristics of the graphene synthesized in this work, this work has implications for applications in graphene-based electronic devices.

Laminated beam specimens were fabricated to mechanically transfer the graphene from a sapphire growth substrate via an epoxy-coated target sapphire strip. A fracture experiment was then used to delaminate the specimens and determine the adhesion energy (2.2 ± 0.4 J/m^2), interfacial strength (3.8 ± 0.4 MPa), and interaction range (1.4 ± 0.3 μm) at the graphene/sapphire interface from a beam-on-elastic foundation model for the load−displacement measurements. Raman analyses confirmed that bilayer graphene had completely delaminated from its donor substrate. Lorentzian deconvolution was used in confirming that the transferred graphene was also bilayer in nature. The quality and yield of the transfer were further evaluated using SEM and AFM microscopy to be about 95%. The cohesive interactions at the graphene/sapphire interface were represented by a bilinear traction−separation relationship that was directly extracted from the data provided by the fracture experiment. The relatively low strength and long range of the graphene/sapphire interaction suggested that mechanisms other than simple van der Waals forces could be present at the interface between graphene and sapphire. It should be noted that the graphene that was transferred to the donor substrate has a layer of epoxy between it and the sapphire, and a second transfer step is required to remove that epoxy.

Two-step, dry transfer processes that rely on delamination require a differential in adhesion properties of graphene interfaces for each step. Varying the rate of separation on the interactions between graphene and polymers has already been identified[14] as one potential tool. The dual actuator loading device will additionally allow mixed-mode interactions to be determined.[40] It is possible that there will be a differential in adhesive interactions over a range of mode-mix values that may also be exploited for the two-step dry transfer. Such rate and mode-mix effects[48] are expected to broaden options for the automation of large wafer-scale transfer of graphene to suitable substrates.

■ ASSOCIATED CONTENT

Supporting Information

The Supporting Information is available free of charge at https://pubs.acs.org/doi/10.1021/acsanm.3c03533.

SEM and optical images of as-grown graphene, XPS measurements of as-grown graphene, Raman spectra, maps and Lorentzian deconvolution of as-grown and transferred samples, stress−strain curve from 3-point bending test on sapphire, displacements and rotations obtained from digital image correlation, adhesion energy and strength data for various specimens tested, comparison table of previous works done on the direct growth of graphene on sapphire, comparison of the growths across different orientations of sapphire, dry transfer data obtained from the literature from previous works on graphene/copper foil (PDF)

■ AUTHOR INFORMATION

Corresponding Author

Kenneth M. Liechti − *Materials Science and Engineering and Texas Materials Institute and Center for Mechanics of Solids, Structures and Materials in the Department of Aerospace Engineering and Engineering Mechanics, University of Texas at Austin, Austin, Texas 78712, United States*; Phone: 512-672-9619; Email: kml@mail.utexas.edu

https://doi.org/10.1021/acsanm.3c03533
ACS Appl. Nano Mater. 2023, 6, 19018−19028

Authors

Sivasakthya Mohan − *Materials Science and Engineering and Texas Materials Institute and Center for Mechanics of Solids, Structures and Materials in the Department of Aerospace Engineering and Engineering Mechanics, University of Texas at Austin, Austin, Texas 78712, United States;* orcid.org/0000-0002-4529-6226

Dmitry Kireev − *Department of Electrical and Computer Engineering, University of Texas at Austin, Austin, Texas 78712, United States; Department of Biomedical Engineering, University of Massachusetts Amherst, Amherst, Massachusetts 01003, United States;* orcid.org/0000-0003-1499-5435

Shanmukh Kutagulla − *Materials Science and Engineering and Texas Materials Institute, University of Texas at Austin, Austin, Texas 78712, United States;* orcid.org/0000-0002-4078-8053

Nicholas Ignacio − *Materials Science and Engineering and Texas Materials Institute, University of Texas at Austin, Austin, Texas 78712, United States;* orcid.org/0000-0001-8663-3033

Yuqian Gu − *Department of Electrical and Computer Engineering, University of Texas at Austin, Austin, Texas 78712, United States;* orcid.org/0000-0003-2673-2712

Hugo Celio − *Materials Science and Engineering and Texas Materials Institute, University of Texas at Austin, Austin, Texas 78712, United States*

Xun Zhan − *Materials Science and Engineering and Texas Materials Institute, University of Texas at Austin, Austin, Texas 78712, United States*

Deji Akinwande − *Materials Science and Engineering and Texas Materials Institute and Department of Electrical and Computer Engineering, University of Texas at Austin, Austin, Texas 78712, United States;* orcid.org/0000-0001-7133-5586

Complete contact information is available at: https://pubs.acs.org/10.1021/acsanm.3c03533

Notes

The authors declare no competing financial interest.

■ ACKNOWLEDGMENTS

The authors gratefully acknowledge the financial support of this work by the National Science Foundation through Grant 2110526 and the Office of Naval Research under Grant N00014-18-1-2706. The work was partly conducted at the Texas Nanofabrication Facility supported by NSF Grant NNCI-2025227.

■ REFERENCES

(1) Bonaccorso, F.; Sun, Z.; Hasan, T.; Ferrari, A. C. Graphene Photonics and Optoelectronics. *Nat. Photonics* **2010**, *4* (9), 611−622.

(2) Akinwande, D.; Brennan, C. J.; Bunch, J. S.; Egberts, P.; Felts, J. R.; Gao, H.; Huang, R.; Kim, J.-S.; Li, T.; Li, Y.; Liechti, K. M.; Lu, N.; Park, H. S.; Reed, E. J.; Wang, P.; Yakobson, B. I.; Zhang, T.; Zhang, Y.-W.; Zhou, Y.; Zhu, Y. A Review on Mechanics and Mechanical Properties of 2D Materials—Graphene and Beyond. *Extreme Mech. Lett.* **2017**, *13*, 42−77.

(3) Soldano, C.; Mahmood, A.; Dujardin, E. Production, Properties and Potential of Graphene. *Carbon* **2010**, *48* (8), 2127−2150.

(4) Novoselov, K. S.; Geim, A. K.; Morozov, S. V.; Jiang, D.; Zhang, Y.; Dubonos, S. V.; Grigorieva, I. V.; Firsov, A. A. Electric Field Effect in Atomically Thin Carbon Films. *Science* **2004**, *306* (5696), 666−669.

(5) Zurutuza, A.; Marinelli, C. Challenges and Opportunities in Graphene Commercialization. *Nat. Nanotechnol.* **2014**, *9* (10), 730−734.

(6) Lin, L.; Peng, H.; Liu, Z. Synthesis Challenges for Graphene Industry. *Nat. Mater.* **2019**, *18* (6), 520−524.

(7) Chen, Y.; Gong, X.; Gai, J. Progress and Challenges in Transfer of Large-Area Graphene Films. *Adv. Sci.* **2016**, *3* (8), 1500343.

(8) Yan, Z.; Lin, J.; Peng, Z.; Sun, Z.; Zhu, Y.; Li, L.; Xiang, C.; Samuel, E. L.; Kittrell, C.; Tour, J. M. Toward the Synthesis of Wafer-Scale Single-Crystal Graphene on Copper Foils. *ACS Nano* **2012**, *6* (10), 9110−9117.

(9) Li, X.; Colombo, L.; Ruoff, R. S. Synthesis of Graphene Films on Copper Foils by Chemical Vapor Deposition. *Adv. Mater.* **2016**, *28* (29), 6247−6252.

(10) Zhang, Y.; Zhang, L.; Zhou, C. Review of Chemical Vapor Deposition of Graphene and Related Applications. *Acc. Chem. Res.* **2013**, *46* (10), 2329−2339.

(11) Cho, J. H.; Na, S. R.; Park, S.; Akinwande, D.; Liechti, K. M.; Cullinan, M. A. Controlling the Number of Layers in Graphene Using the Growth Pressure. *Nanotechnology* **2019**, *30* (23), 235602.

(12) Lupina, G.; Kitzmann, J.; Costina, I.; Lukosius, M.; Wenger, C.; Wolff, A.; Vaziri, S.; Östling, M.; Pasternak, I.; Krajewska, A.; Strupinski, W.; Kataria, S.; Gahoi, A.; Lemme, M. C.; Ruhl, G.; Zoth, G.; Luxenhofer, O.; Mehr, W. Residual Metallic Contamination of Transferred Chemical Vapor Deposited Graphene. *ACS Nano* **2015**, *9* (5), 4776−4785.

(13) Yoon, T.; Shin, W. C.; Kim, T. Y.; Mun, J. H.; Kim, T.-S.; Cho, B. J. Direct Measurement of Adhesion Energy of Monolayer Graphene As-Grown on Copper and Its Application to Renewable Transfer Process. *Nano Lett.* **2012**, *12* (3), 1448−1452.

(14) Na, S. R.; Suk, J. W.; Tao, L.; Akinwande, D.; Ruoff, R. S.; Huang, R.; Liechti, K. M. Selective Mechanical Transfer of Graphene from Seed Copper Foil Using Rate Effects. *ACS Nano* **2015**, *9* (2), 1325−1335.

(15) Hong, N.; Zhao, Q.; Chen, D.; Liechti, K. M.; Li, W. A Method to Estimate Adhesion Energy of As-Grown Graphene in a Roll-to-Roll Dry Transfer Process. *Carbon* **2023**, *201*, 712−718.

(16) Na, S. R.; Rahimi, S.; Tao, L.; Chou, H.; Ameri, S. K.; Akinwande, D.; Liechti, K. M. Clean Graphene Interfaces by Selective Dry Transfer for Large Area Silicon Integration. *Nanoscale* **2016**, *8* (14), 7523−7533.

(17) Tao, L.; Lee, J.; Chou, H.; Holt, M.; Ruoff, R. S.; Akinwande, D. Synthesis of High Quality Monolayer Graphene at Reduced Temperature on Hydrogen-Enriched Evaporated Copper (111) Films. *ACS Nano* **2012**, *6* (3), 2319−2325.

(18) Cho, J. H.; Gorman, J. J.; Na, S. R.; Cullinan, M. Growth of Monolayer Graphene on Nanoscale Copper-Nickel Alloy Thin Films. *Carbon* **2017**, *115*, 441−448.

(19) Lukosius, M.; Dabrowski, J.; Kitzmann, J.; Fursenko, O.; Akhtar, F.; Lisker, M.; Lippert, G.; Schulze, S.; Yamamoto, Y.; Schubert, M. A.; Krause, H. M.; Wolff, A.; Mai, A.; Schroeder, T.; Lupina, G. Metal-Free CVD Graphene Synthesis on 200 Mm Ge/Si(001) Substrates. *ACS Appl. Mater. Interfaces* **2016**, *8* (49), 33786−33793.

(20) Kim, H.; Song, I.; Park, C.; Son, M.; Hong, M.; Kim, Y.; Kim, J. S.; Shin, H.-J.; Baik, J.; Choi, H. C. Copper-Vapor-Assisted Chemical Vapor Deposition for High-Quality and Metal-Free Single-Layer Graphene on Amorphous SiO_2 Substrate. *ACS Nano* **2013**, *7* (8), 6575−6582.

(21) Vishwakarma, R.; Rosmi, M. S.; Takahashi, K.; Wakamatsu, Y.; Yaakob, Y.; Araby, M. I.; Kalita, G.; Kitazawa, M.; Tanemura, M. Transfer Free Graphene Growth on SiO_2 Substrate at 250 °C. *Sci. Rep.* **2017**, *7* (1), 43756.

(22) Muñoz, R.; Munuera, C.; Martínez, J. I.; Azpeitia, J.; Gómez-Aleixandre, C.; García-Hernández, M. Low Temperature Metal Free Growth of Graphene on Insulating Substrates by Plasma Assisted Chemical Vapor Deposition. *2D Mater.* **2017**, *4* (1), No. 015009.

(23) Norimatsu, W.; Kusunoki, M. Epitaxial Graphene on SiC{0001}: Advances and Perspectives. *Phys. Chem. Chem. Phys.* **2014**, *16* (8), 3501.

(24) Mishra, N.; Boeckl, J.; Motta, N.; Iacopi, F. Graphene Growth on Silicon Carbide: A Review. *Phys. Status Solidi A* **2016**, *213* (9), 2277−2289.
(25) Yazdi, G. R.; Iakimov, T.; Yakimova, R. Epitaxial Graphene on SiC: A Review of Growth and Characterization. *Crystals* **2016**, *6* (5), 53.
(26) Tai, L.; Zhu, D.; Liu, X.; Yang, T.; Wang, L.; Wang, R.; Jiang, S.; Chen, Z.; Xu, Z.; Li, X. Direct Growth of Graphene on Silicon by Metal-Free Chemical Vapor Deposition. *Nano-Micro Lett.* **2018**, *10* (2), 20.
(27) Lin, M.-Y.; Su, C.-F.; Lee, S.-C.; Lin, S.-Y. The Growth Mechanisms of Graphene Directly on Sapphire Substrates by Using the Chemical Vapor Deposition. *J. Appl. Phys.* **2014**, *115* (22), 223510.
(28) Fanton, M. A.; Robinson, J. A.; Puls, C.; Liu, Y.; Hollander, M. J.; Weiland, B. E.; LaBella, M.; Trumbull, K.; Kasarda, R.; Howsare, C.; Stitt, J.; Snyder, D. W. Characterization of Graphene Films and Transistors Grown on Sapphire by Metal-Free Chemical Vapor Deposition. *ACS Nano* **2011**, *5* (10), 8062−8069.
(29) Mishra, N.; Forti, S.; Fabbri, F.; Martini, L.; McAleese, C.; Conran, B. R.; Whelan, P. R.; Shivayogimath, A.; Jessen, B. S.; Buß, L.; Falta, J.; Aliaj, I.; Roddaro, S.; Flege, J. I.; Bøggild, P.; Teo, K. B. K.; Coletti, C. Wafer-Scale Synthesis of Graphene on Sapphire: Toward Fab-Compatible Graphene. *Small* **2019**, *15* (50), 1904906.
(30) Li, J.; Chen, M.; Samad, A.; Dong, H.; Ray, A.; Zhang, J.; Jiang, X.; Schwingenschlögl, U.; Domke, J.; Chen, C.; Han, Y.; Fritz, T.; Ruoff, R. S.; Tian, B.; Zhang, X. Wafer-Scale Single-Crystal Monolayer Graphene Grown on Sapphire Substrate. *Nat. Mater.* **2022**, *21* (7), 740−747.
(31) Dou, Z.; Chen, Z.; Li, N.; Yang, S.; Yu, Z.; Sun, Y.; Li, Y.; Liu, B.; Luo, Q.; Ma, T.; Liao, L.; Liu, Z.; Gao, P. Atomic Mechanism of Strong Interactions at the Graphene/Sapphire Interface. *Nat. Commun.* **2019**, *10* (1), 5013.
(32) Kang, L.; Tian, D.; Meng, L.; Du, M.; Yan, W.; Meng, Z.; Li, X. Epitaxial Growth of Highly-Aligned MoS2 on c-Plane Sapphire. *Surf. Sci.* **2022**, *720*, 122046.
(33) Malard, L. M.; Pimenta, M. A.; Dresselhaus, G.; Dresselhaus, M. S. Raman Spectroscopy in Graphene. *Phys. Rep.* **2009**, *473* (5−6), 51−87.
(34) Childres, I.; Jauregui, L. A.; Park, W.; Cao, H.; Chen, Y. P. Raman Spectroscopy of Graphene and Related Materials. *New developments in photon and materials research*, 2013, *1*, pp.1−20.
(35) Zhu, W.; Low, T.; Perebeinos, V.; Bol, A. A.; Zhu, Y.; Yan, H.; Tersoff, J.; Avouris, P. Structure and Electronic Transport in Graphene Wrinkles. *Nano Lett.* **2012**, *12* (7), 3431−3436.
(36) Chang, C.-J.; Tsai, P.-C.; Su, W.-Y.; Huang, C.-Y.; Lee, P.-T.; Lin, S.-Y. Layered Graphene Growth Directly on Sapphire Substrates for Applications. *ACS Omega* **2022**, *7* (15), 13128−13133.
(37) Chen, Z.; Xie, C.; Wang, W.; Zhao, J.; Liu, B.; Shan, J.; Wang, X.; Hong, M.; Lin, L.; Huang, L.; Lin, X.; Yang, S.; Gao, X.; Zhang, Y.; Gao, P.; Novoselov, K. S.; Sun, J.; Liu, Z. Direct Growth of Wafer-Scale Highly Oriented Graphene on Sapphire. *Sci. Adv.* **2021**, *7* (47), eabk0115.
(38) Losurdo, M.; Giangregorio, M. M.; Capezzuto, P.; Bruno, G. Graphene CVD Growth on Copper and Nickel: Role of Hydrogen in Kinetics and Structure. *Phys. Chem. Chem. Phys.* **2011**, *13* (46), 20836.
(39) Komurasaki, H.; Isono, T.; Tsukamoto, T.; Ogino, T. Evolution of Step Morphology on Vicinal Sapphire (1 − 1 0 2) Surfaces Accompanied with Self-Assembly of Comb-Shaped Chemical Domains. *Appl. Surf. Sci.* **2012**, *258* (15), 5666−5671.
(40) Yang, T.; Yang, X.; Huang, R.; Liechti, K. M. Rate-Dependent Traction-Separation Relations for a Silicon/Epoxy Interface Informed by Experiments and Bond Rupture Kinetics. *J. Mech. Phys. Solids* **2019**, *131*, 1−19.
(41) Jain, S.; Liechti, K. M.; Bonnecaze, R. T. Cohesive Zone Models to Understand the Interface Mechanics of Thin Film Transfer Printing. *J. Appl. Phys.* **2019**, *125* (7), No. 075301.
(42) Al-Muhit, B.; Sanchez, F. Traction-Separation Response of Bilayer Graphene Interfaces: The Role of an Intercalated Single Atomic Layer of Water Molecules and Hydroxyl Groups. *Appl. Surf. Sci.* **2021**, *540*, 148280.
(43) Gould, T.; Liu, Z.; Liu, J. Z.; Dobson, J. F.; Zheng, Q.; Lebègue, S. Binding and Interlayer Force in the Near-Contact Region of Two Graphite Slabs: Experiment and Theory. *J. Chem. Phys.* **2013**, *139* (22), 224704.
(44) Li, B.; Yin, J.; Liu, X.; Wu, H.; Li, J.; Li, X.; Guo, W. Probing van Der Waals Interactions at Two-Dimensional Heterointerfaces. *Nat. Nanotechnol.* **2019**, *14* (6), 567−572.
(45) Kireev, D.; Brambach, M.; Seyock, S.; Maybeck, V.; Fu, W.; Wolfrum, B.; Offenhäusser, A. Graphene Transistors for Interfacing with Cells: Towards a Deeper Understanding of Liquid Gating and Sensitivity. *Sci. Rep.* **2017**, *7* (1), 6658.
(46) Kireev, D.; Ameri, S. K.; Nederveld, A.; Kampfe, J.; Jang, H.; Lu, N.; Akinwande, D. Fabrication, Characterization and Applications of Graphene Electronic Tattoos. *Nat. Protoc.* **2021**, *16* (5), 2395−2417.
(47) Gammelgaard, L.; Caridad, J. M; Cagliani, A.; Mackenzie, D. M A; Petersen, D. H; Booth, T. J; Bøggild, P. Graphene Transport Properties upon Exposure to PMMA Processing and Heat Treatments. *2D Mater.* **2014**, *1* (3), No. 035005.
(48) Yang, T.; Gandhi, V.; Huang, R.; Liechti, K. M. Rate Dependent Fracture along a Silicon/Epoxy Interface under Mixed-Mode Loading Conditions. *Int. J. Solids Struct.* **2022**, *257*, 111129.

https://doi.org/10.1021/acsanm.3c03533
ACS Appl. Nano Mater. 2023, 6, 19018−19028